



ELSEVIER

Contents lists available at ScienceDirect

## International Journal of Non-Linear Mechanics

journal homepage: [www.elsevier.com/locate/nlm](http://www.elsevier.com/locate/nlm)

# Nonlocal continuum model for large deformation analysis of SLGSs using the kp-Ritz element-free method



Yang Zhang<sup>a,b</sup>, L.W. Zhang<sup>c,\*</sup>, K.M. Liew<sup>a,d</sup>, J.L. Yu<sup>b</sup>

<sup>a</sup> Department of Architecture and Civil Engineering, City University of Hong Kong, Kowloon, Hong Kong SAR

<sup>b</sup> CAS Key Laboratory of Mechanical Behavior and Design of Materials, University of Science and Technology of China, Hefei, China

<sup>c</sup> College of Information Science and Technology, Shanghai Ocean University, Shanghai 201306, China

<sup>d</sup> City University of Hong Kong Shenzhen Research Institute Building, Shenzhen Hi-Tech Industrial Park, Nanshan District, Shenzhen, China

## ARTICLE INFO

### Article history:

Received 1 May 2015

Received in revised form

31 October 2015

Accepted 1 November 2015

Available online 10 November 2015

### Keywords:

Element-free kp-Ritz method

Nonlinear large deformation

SLGSs

Nonlocal elasticity theory

## ABSTRACT

A geometrically nonlinear large deformation analysis of SLGSs is presented using the element-free kp-Ritz method. Classical plate theory (CLP) is applied to describe the geometrically nonlinear behavior of SLGSs. Nonlocal elasticity theory is incorporated into CLP to take the small-scale effect into consideration. The system nonlinear equations are derived from the Ritz procedure based on the total Lagrangian formulation. The modified Newton–Raphson method and arc-length continuation are employed to solve the nonlinear equations. The efficiency of the element-free kp-Ritz method is verified through comparison with results reported in previous research. Numerical cases are studied to examine the influence of boundary conditions, aspect ratio, side length and nonlocal parameters on the nonlinear large deformation behavior of SLGSs. An interesting phenomenon is observed in that the nonlocal parameter effect is related to the mathematical expression of the transverse load.

© 2015 Elsevier Ltd. All rights reserved.

## 1. Introduction

Benzene-ring structure packed single layered carbon atoms, known as single layered graphene sheets (SLGSs), have attracted considerable attention in the scientific community since the emergence of the groundbreaking paper written by Novoselov et al. [1], due to its excellent mechanical, electronic, magnetic, thermal, physical and chemical properties [2–5]. It has wide applications in nano-electro-mechanical systems (NEMS) and macro-electro-mechanical systems (MEMS), including the fields of nanosensors, nanodevices, nanoelectronics etc. Many carbon-based materials, including nanotubes, graphite, fullerenes, etc., can be recognized as derivations of SLGSs [6]. Thus, as mechanics researchers, we are strongly motivated to gain a greater understanding of the mechanical properties of SLGSs.

While it is difficult to conduct experiments for the study of nanoscale structures, simulations have become the dominant tool with which to investigate the mechanical properties of nanoscale structures. Generally, simulations contain three categories, i.e. bottom-up simulations, the hybrid of bottom-up simulations and top-down simulations. Atomistic lattice dynamics and molecular dynamic simulations [7,8] belong to bottom-up simulations and

require such a tremendous amount of computation that they are limited to structures with small numbers of atoms and molecules. In the case of hybrid simulations, although the complexity of the problem processing increases, a lesser degree of computation is demanded compared to bottom-up simulations. Continuum modeling simulations [9–11] belong to top-down simulations, offering the least computationally expensive option. Therefore, continuum modelling simulations have been increasingly applied in the study of nanoscale structures. However, original continuum modelling cannot be used directly because it lacks the ability to capture the small-scale effect. The small-scale effect results from the not inconsiderable forces between individual atoms when the structures are small in size. Consequently, modified continuum modelling is needed to take the small-scale effect into account. Generally, the nonlocal elasticity theory is incorporated to modify continuum modelling. The nonlocal elasticity theory, developed by Eringen [12,13], has the ability to capture the small-scale effect on account of its assumption that the stress state at a given reference point has a relationship with the strain of every point in the body, rather than just with the reference point. Such nonlocal continuum modelling was first employed by Peddieson [14] to study some representative problems of beams by formulating a nonlocal version of the Bernoulli/Euler beam theory. Wave propagation in CNTs was investigated by Wang [15], using the nonlocal Euler–Bernoulli and Timoshenko beam models. Arash developed the nonlocal finite element method to study the wave propagation

\* Corresponding author.

E-mail address: [lwzhang@shou.edu.cn](mailto:lwzhang@shou.edu.cn) (L.W. Zhang).

behavior of graphene sheets [16]. Rouhi et al. [17] applied the atomistic finite element model to an analysis of the axial buckling behavior of SLGSs. Zhang et al. [18,19] adopted the nonlocal plate model to investigate the vibration behavior and transient response of SLGSs. It is indicated that nonlocal continuum modelling is effective in dealing with various problems of nanoscale structures.

Nonlocal continuum modelling for a featured problem is followed by a numerical solving process. As a notable numerical tool, the element-free  $kp$ -Ritz method has proved effective and efficient in analyzing extensive problems in the field of engineering [20–25] due to its distinguished feature of not relying on mesh, a feature which makes it especially good at processing nonlinear problems (e.g. geometrically nonlinear problems [26]).

Many researchers have employed nonlocal continuum modelling to investigate the nonlinear behavior of graphene sheets. Naderi [27] employed nonlocal continuum modelling and the Galerkin method to analyze the postbuckling of graphene sheets in a nonlinear polymer medium. Nonlocal continuum modelling was utilized by Jomehzadeh [28] to investigate the large amplitude vibration characteristics of multilayered graphene sheets and a numerical solution was obtained based on the harmonic balance method. The nonlinear bending behavior of SLGSs has been investigated in a few papers [29,30]. Jomehzadeh et al. [31] analytically calculated the softening and hardening bending stiffness of a monolayer graphene sheet with an initial curvature and found that the bending stiffness strongly depends on the initial configuration; however, to the author's best knowledge, no work exists on the large deformation behavior of SLGSs employing the element-free  $kp$ -Ritz method.

In this paper, we aim to provide a comprehensive investigation of the large deformation behavior of SLGSs using nonlocal continuum modelling and the element-free  $kp$ -Ritz method. The effect of the boundary conditions, aspect ratio, side length and nonlocal parameters are studied.

## 2. Nonlocal continuum formulation for the large deformation of SLGSs

### 2.1. Nonlocal elasticity theory

Inspired by experimental observation and the atomic theory of lattice dynamics, Eringen [12,13] recognized that the stress state in the prescribed point depends not only on the strain state of the same point but also on that of all the other points in the body. Thus, he presented the nonlocal elasticity theory to describe this insight. The key issue of the nonlocal elasticity theory lies in the distinct description of the constitutive relation. The most widely applied constitutive relation is written in the following differential form

$$(1 - (e_0 a)^2 \nabla^2) \vec{\sigma}_{nl} = C : \vec{\epsilon}, \quad (1)$$

where  $e_0 a$  is the nonlocal parameter reflecting the small-scale effect,  $\nabla^2$  denotes the Laplacian operator equaling  $(\partial/\partial x^2 + \partial/\partial y^2)$  and  $C$  is the modulus tensor.

### 2.2. Total potential energy

Based on the Von Karman theory and Ritz method, a formulation for the large deformation analysis of SLGSs is derived. The displacement field in Von Karman theory is expressed as [32]

$$u(x, y, z) = u_0(x, y) - z \frac{\partial w_0}{\partial x},$$

$$v(x, y, z) = v_0(x, y) - z \frac{\partial w_0}{\partial y},$$

$$w(x, y, z) = w_0(x, y), \quad (2)$$

where  $(u, v, w)$  are the displacements of arbitrary point  $(x, y, z)$  in the SLGSs and  $u_0, v_0, w_0$  denote the displacements of a point on the mid-plane. For geometrically nonlinear analyses, the nonlinear terms are considered through the nonlinear formulation of strains, which are written as

$$\vec{\epsilon} = \begin{bmatrix} \epsilon_{xx} \\ \epsilon_{yy} \\ \gamma_{xy} \end{bmatrix} = \vec{\epsilon}_L + \vec{\kappa} + \vec{\epsilon}_N = \begin{bmatrix} \frac{\partial u}{\partial x} \\ \frac{\partial v}{\partial y} \\ \frac{\partial u}{\partial y} + \frac{\partial v}{\partial x} \end{bmatrix} + \begin{bmatrix} -z \frac{\partial^2 w}{\partial x^2} \\ -z \frac{\partial^2 w}{\partial y^2} \\ -2z \frac{\partial^2 w}{\partial xy} \end{bmatrix} + \begin{bmatrix} \frac{1}{2} (\frac{\partial w}{\partial x})^2 \\ \frac{1}{2} (\frac{\partial w}{\partial y})^2 \\ \frac{\partial w}{\partial x} \frac{\partial w}{\partial y} \end{bmatrix}. \quad (3)$$

Thus, the nonlocal constitutive relation for SLGSs can be expressed as

$$(1 - (e_0 a)^2 \nabla^2) \vec{\sigma}_{nl} = S \cdot \vec{\epsilon}, \quad (4)$$

$$S = \begin{bmatrix} E/(1 - \nu^2) & \nu E/(1 - \nu^2) & 0 \\ \nu E/(1 - \nu^2) & E/(1 - \nu^2) & 0 \\ 0 & 0 & E/(2(1 + \nu)) \end{bmatrix}, \quad (5)$$

where  $E, \nu$  denote Young's modulus and Poisson's ratio, respectively.

The strain energy of SLGSs is expressed as

$$U_\epsilon = \frac{1}{2} \int_{\Omega} \vec{\sigma}_{nl}^T \cdot \vec{\epsilon} d\Omega. \quad (6)$$

Taking the transverse load into consideration, the external work is written as

$$W = \iint w q dx dy, \quad (7)$$

and, thus, we can obtain the total potential energy of SLGSs

$$\Pi = U - W = \frac{1}{2} \int_{\Omega} \vec{\sigma}_{nl}^T \cdot \vec{\epsilon} d\Omega - \iint w q dx dy. \quad (8)$$

Taking the variation of the total potential energy functional, the following equilibrium equation is yielded

$$\int_{\Omega} \vec{\sigma}_{nl}^T \cdot \delta \vec{\epsilon} d\Omega - \iint q \delta w dx dy = 0, \quad (9)$$

and by multiplying Eq. (9) with  $(1 - (e_0 a)^2 \nabla^2)$  and substituting Eqs. (3) and (4) into (9), we can get

$$\int_{\Omega} (\vec{\epsilon}_L^T S \delta \vec{\epsilon}_L + \vec{\epsilon}_L^T S \delta \vec{\kappa} + \vec{\kappa}^T S \delta \vec{\epsilon}_L + \vec{\kappa}^T S \delta \vec{\kappa}) d\Omega + \int_{\Omega} (\vec{\epsilon}_N^T S \delta \vec{\epsilon}_N + \vec{\kappa}^T S \delta \vec{\epsilon}_N + \vec{\epsilon}_N^T S \delta \vec{\epsilon}_L + \vec{\epsilon}_N^T S \delta \vec{\kappa} + \vec{\epsilon}_N^T S \delta \vec{\epsilon}_N) d\Omega - \iint (1 - (e_0 a)^2 \nabla^2) q \delta w dx dy = 0. \quad (10)$$

### 2.3. Discretized nonlinear equations from the Ritz procedure

The displacement field of SLGSs can be expressed using  $N$  displacement values of the scattered particles  $(\vec{X}_1, \vec{X}_2, \dots, \vec{X}_N)$  according to the kernel particle Ritz method, as follows

$$w = \sum_{I=1}^N \psi_I(x, y) w_I, \quad (11)$$

where  $N$  is the total number of nodes used to discretize the domain.  $\psi_I$  and  $w_I$  denote the shape function and displacement value associated with node  $I$ , respectively.

The shape function can be expressed by

$$\psi_I = C(\vec{X}; \vec{X} - \vec{X}_I) \Phi(\vec{X} - \vec{X}_I), \quad (12)$$

in which,  $\Phi(\vec{X} - \vec{X}_i)$  is the kernel function. The coefficient function  $C(\vec{X}; \vec{X} - \vec{X}_i)$  is defined as

$$C(\vec{X}; \vec{X} - \vec{X}_i) = H^T(\vec{X} - \vec{X}_i)K(\vec{X}), \quad (13)$$

$$H^T(\vec{X} - \vec{X}_i) = [1, x - x_i, y - y_i, (x - x_i)(y - y_i), (x - x_i)^2, (y - y_i)^2]^T, \quad (14)$$

$$K(\vec{X}) = [k_0(x, y), k_1(x, y), k_2(x, y), k_3(x, y), k_4(x, y), k_5(x, y)]^T, \quad (15)$$

where  $H$  is the quadratic basis vector and  $K(\vec{X})$  is the function of  $\vec{X}$  which needs to be determined. Thus, we can rewrite the shape function as

$$\psi_i(\vec{X}; \vec{X} - \vec{X}_i) = K^T(\vec{X})H(\vec{X} - \vec{X}_i)\Phi(\vec{X} - \vec{X}_i) \quad (16)$$

When we force the shape function to satisfy the reproduction conditions

$$\sum_{i=1}^N \psi_i(\vec{X})x_i^p y_i^q \quad \text{for } p+q=0, 1, 2., \quad (17)$$

we can obtain

$$K(\vec{X}) = M^{-1}(\vec{X})H(0), \quad (18)$$

in which

$$M(\vec{X}) = \sum_{i=1}^N H(\vec{X} - \vec{X}_i)H^T(\vec{X} - \vec{X}_i)\Phi(\vec{X} - \vec{X}_i), \quad (19)$$

$$H(0) = [1, 0, 0, 0, 0, 0]^T \quad (20)$$

In addition, the kernel function is expressed as

$$\Phi(\vec{X} - \vec{X}_i) = \Phi(x; x_i) \cdot \Phi(y; y_i), \quad (21)$$

where

$$\Phi(x; x_i) = \phi\left(\frac{|x - x_i|}{a_i}\right) \quad (22)$$

In the present study, the cubic spline function is employed for the kernel function

$$\phi(z_i) = \begin{cases} \frac{2}{3} - 4z_i^2 + 4z_i^3 & \text{for } 0 \leq z_i \leq \frac{1}{2} \\ \frac{4}{3} - 4z_i + 4z_i^2 - \frac{4}{3}z_i^3 & \text{for } \frac{1}{2} \leq z_i \leq 1, \\ 0 & \text{otherwise} \end{cases} \quad (23)$$

in which  $z_i = |x - x_i|/a_i$  and  $a_i = a(x_i)$  are the dilation parameters used to control the size of the support area of node  $i$ , i.e. the subdomain in which  $\Phi(x_j; x_i) \neq 0$  for all nodes  $x_j$ . Generally,  $a_i$  is defined as  $d_{\max}c_i$ .  $d_{\max}$  is the scaling factor spanning from 2.0 to 4.0, which should be appropriately selected so as to ensure the support area contains a sufficient number of nodes, thereby avoiding the singularity of the matrix  $M$ .  $c_i$  is the larger of the distances between the two neighbors and  $x_i$ .

Based on the assumptions of displacements as described in Eq. (11), the strain of SLGSs can be written as

$$\vec{\epsilon} = \vec{\epsilon}_L + \vec{\kappa} + \vec{\epsilon}_N = \sum_{i=1}^N B_i^L \begin{bmatrix} u_i \\ v_i \end{bmatrix} + \sum_{i=1}^N \begin{bmatrix} -z\psi_{i,xx} \\ -z\psi_{i,xy} \\ -2z\psi_{i,xy} \end{bmatrix} w_i + \begin{bmatrix} \frac{1}{2} \left( \sum_{i=1}^N \psi_{i,x} w_i \right)^2 \\ \frac{1}{2} \left( \sum_{i=1}^N \psi_{i,y} w_i \right)^2 \\ \left( \sum_{i=1}^N \psi_{i,x} w_i \right) \cdot \left( \sum_{i=1}^N \psi_{i,y} w_i \right) \end{bmatrix}, \quad (24)$$

where

$$B_i^L = \begin{bmatrix} \psi_{i,x} & 0 \\ 0 & \psi_{i,y} \\ \psi_{i,y} & \psi_{i,x} \end{bmatrix}. \quad (25)$$

Substituting Eq. (24) into Eq. (10), we can obtain the discretized equilibrium system equations

$$K_s(\mathbf{u})\mathbf{u} = F, \quad (26)$$

in which  $\mathbf{u} = [u_1, v_1, w_1, \dots, u_N, v_N, w_N]$  and  $K_s$  is the secant stiffness matrix depending on the displacement. It contains two parts

$$K_s(\mathbf{u}) = K^L + K^N(\mathbf{u}), \quad (27)$$

and

$$K_{ij}^L = \iint \begin{bmatrix} (B_i^L)^T A B_j^L & (B_i^L)^T B B_j^K \\ (B_i^K)^T B B_j^L & (B_i^K)^T Q B_j^K \end{bmatrix} dx dy$$

$$K_{ij}^N = \iint \begin{bmatrix} 0 & \frac{1}{2}(B_i^L)^T A B_j^N \\ (B_i^N)^T A B_j^L & \frac{1}{2}(B_i^N)^T B B_j^N + (B_i^K)^T B B_j^N + \frac{1}{2}(B_i^N)^T A B_j^N \end{bmatrix} dx dy, \quad (28)$$

$$(A, B, Q) = \int_{-h/2}^{h/2} S(1, z, z^2) dz, \quad (29)$$

$$B_i^L = \begin{bmatrix} \psi_{i,x} & 0 \\ 0 & \psi_{i,y} \\ \psi_{i,y} & \psi_{i,x} \end{bmatrix}, B_i^K = \begin{bmatrix} -\psi_{i,xx} \\ -\psi_{i,yy} \\ -2\psi_{i,xy} \end{bmatrix}, B_i^N = \begin{bmatrix} \frac{\partial w}{\partial x} \psi_{i,x} \\ \frac{\partial w}{\partial y} \psi_{i,y} \\ \frac{\partial w}{\partial y} \psi_{i,x} + \frac{\partial w}{\partial x} \psi_{i,y} \end{bmatrix}, \quad (30)$$

$$F_i = \iint (1 - (e_0 a)^2 \nabla^2) q \psi_i dx dy \quad (31)$$

The tangent stiffness matrix can be obtained from

$$K_t(\vec{w}) = K^L + K^{Nt} + K^G, \quad (32)$$

$$K_{ij}^{Nt} = \iint \begin{bmatrix} 0 & (B_i^L)^T A B_j^N \\ (B_i^N)^T A B_j^L & (B_i^N)^T B B_j^N + (B_i^K)^T B B_j^N + (B_i^N)^T A B_j^N \end{bmatrix} dx dy$$

$$K_{ij}^G = \iint G_i^T N_j^T dx dy, \quad (33)$$

$$G = \begin{bmatrix} \psi_{i,x} \\ \psi_{i,y} \end{bmatrix}, N = \begin{bmatrix} N_{xx} & N_{xy} \\ N_{xy} & N_{yy} \end{bmatrix}, \begin{bmatrix} N_{xx} \\ N_{yy} \\ N_{xy} \end{bmatrix} = \int_{-h/2}^{h/2} \begin{bmatrix} \sigma_{xx} \\ \sigma_{yy} \\ \sigma_{xy} \end{bmatrix} dz \quad (34)$$

### 3. Solution of discretized nonlinear equations

For solving the nonlinear equations, incremental-iterative methods should be employed. In the present work, the modified Newton–Raphson iteration scheme, combined with the arc-length method, is applied to obtain the nonlinear solutions [33,34]. A detailed figure of the adopted method is presented as follows.

A simple and unadorned supposition emerges that the nonlinear equations can be solved step by step, as follows

$$K_t \cdot \Delta \vec{w}_m = \Delta F_m, \quad (35)$$

where  $K_t$  is the tangent stiffness matrix. However, the solution is not converged. To guarantee solutions on the true equilibrium curve, the Newton–Raphson (NR) iteration scheme is required. Further, in order to reduce the computation load, a modified NR iteration scheme is employed, in which the tangent stiffness matrix is only calculated at the beginning of each step. Fig. 1 illustrates the difference that exists between the standard NR and a modified NR, using a one-dimensional case for simplicity. We

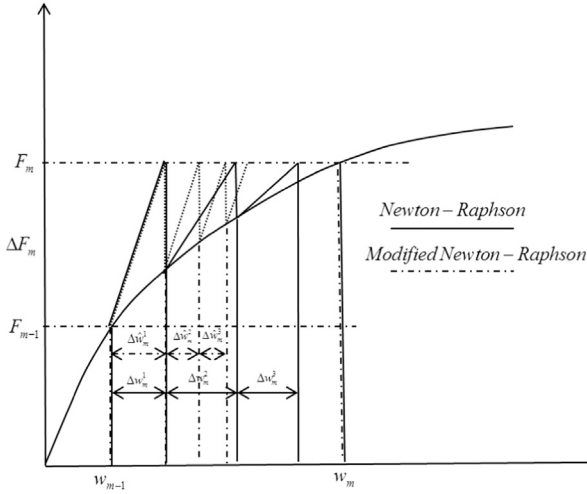


Fig. 1. The comparison between Newton-Raphson and modified Newton-Raphson method.

can obtain the incremental displacement

$$\Delta w_m^n = [K_t(w_{m-1})]^{-1} \{ \Delta F_m - [K_s(w_{m-1})w_m^{n-1} - F_{m-1}] \} \quad (36)$$

However, the deficiency of this method rests in its lack of ability and/or the considerable computation cost required to obtain a response curve with a singular point. To overcome such shortcomings, the arc-length method is introduced in which the response path through a converged solution is achieved at each step.

The basic idea of the arc-length method is to make the convergence controllable by introducing the load scaling factor  $\lambda$  as follows

$$K_s(\vec{w})\vec{w} = \lambda F_0 \quad (37)$$

In this method, both the load and the displacement vary.

According to Liew [33], the incremental displacement is expressed as

$$\begin{aligned} \Delta \vec{w}_m^n &= [K_t(\vec{w}_{m-1})]^{-1} \left\{ \Delta \lambda_m^n F_0 - [K_s(\vec{w}_{m-1})\vec{w}_{m-1}^{n-1} - \lambda_m^{n-1} F_0] \right\} \\ &= \Delta \lambda_m^n (\vec{w}_f)_m - [K_t(\vec{w}_{m-1})]^{-1} g_m^{n-1}, \end{aligned} \quad (38)$$

where  $m$  denotes the load step (the process from the last point of converged equilibrium on the response curve to the current one is known as one load step) number and  $n$  refers to the  $n$ th iteration cycle.  $g_m^{n-1}$  is the residual function, and

$$\begin{aligned} (\vec{w}_f)_m &= [K_t(\vec{w}_{m-1})]^{-1} F_0; \\ g_m^{n-1} &= [K_t(\vec{w}_{m-1})]^{-1} [K_s(\vec{w}_{m-1})\vec{w}_{m-1}^{n-1} - \lambda_m^{n-1} F_0]; \\ \vec{w}_m &= \sum_{i=1}^m \Delta \vec{w}_i, \Delta \vec{w}_i = \sum_{j=1}^N \Delta \vec{w}_i^j, \vec{w}_m^n = \vec{w}_{m-1} + \sum_{k=1}^n \Delta \vec{w}_m^k; \\ \lambda_m &= \sum_{i=1}^m \Delta \lambda_i, \Delta \lambda_i = \sum_{j=1}^N \Delta \lambda_i^j, \lambda_m^n = \lambda_{m-1} + \sum_{k=1}^n \Delta \lambda_m^k, \end{aligned} \quad (39)$$

in which  $N$  is the total iteration number in the  $i$ th load step.

Thus, the key issue lies in solving  $\Delta \lambda_m^n$ . An additional constraint equation is required to obtain  $\Delta \lambda_m^n$ . According to Crisfield [35], the arc-length constraint equation, which guarantees the solution of each iteration located on the “circular arc”, is written as

$$(\Delta \vec{w}_m^n + \sum_{k=1}^{n-1} \Delta \vec{w}_m^k)^T (\Delta \vec{w}_m^n + \sum_{k=1}^{n-1} \Delta \vec{w}_m^k) = l_m^2 \quad (40)$$

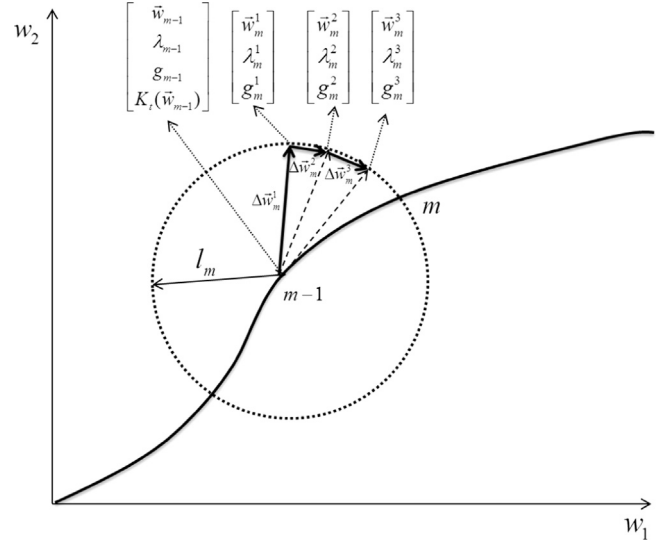


Fig. 2. The process of arc-length method.

Substituting Eq. (37) into Eq. (39), we can get  $\Delta \lambda_m^n$ . Since Eq. (39) may have two roots, the appropriate selection is made according to the least positive cosine value of the angle between  $\sum_{k=1}^{n-1} \Delta \vec{w}_m^k$  and  $\sum_{k=1}^n \Delta \vec{w}_m^k$ .

The procedure contains two parts, i.e. load step-load step evolution and inner load step iteration, which are illustrated in Fig. 2 using a two-dimensional case as an example.

To start the procedure, we need to know the first load increment  $\Delta \lambda_1^1$ . This is usually selected at 20–40% of the anticipated maximum load.

As for load step-load step evolution, the value of  $l_m$  is required

$$l_m^2 = (\Delta \lambda_m^1)^2 (\vec{w}_f)_m^T (\vec{w}_f)_m \quad (41)$$

Then the recursion formula of arc-length can be written

$$l_m = l_{m-1} \left( \frac{J_{des}}{J_{m-1}} \right)^t, \quad (42)$$

where, usually,  $t$  is (0.5~1).  $J_{des}$  denotes the desired number of current inner load step iterations, which is usually taken as (3–5), and  $J_{m-1}$  is the number of the previous inner load step iteration.

$\Delta \lambda_m^1$  is required to get the current inner load step iterations started

$$\Delta \lambda_m^1 = \frac{l_m}{\sqrt{(\vec{w}_f)_m^T (\vec{w}_f)_m}} \cdot \frac{\text{sign}(K_t(\vec{w}_{m-1})) \cdot \text{sign}(\Delta \lambda_{m-1}^1)}{\text{sign}(K_t(\vec{w}_{m-2}))} \quad (43)$$

When  $\|g_m^n\|_2 \leq \beta \|\lambda_m^n F_0\|_2$ , the inner load step iteration ends.

## 4. Numerical results and discussion

### 4.1. Convergence and verification study

Firstly, in order to determine the suitable nodes, and verify the present element-free kp-Ritz method, a convergence and comparison study is carried out. The scaling factor is taken as 2.3. An isotropic, square plate subjected to a uniformly distributed load  $q$  is considered. This example was investigated by Reddy [36] using the finite element method. The side length and thickness are  $a = b = 10$  in and  $h = 1$  in, respectively. Young's modulus and Poisson's ratio are  $E = 7.8 \times 10^6$  psi and  $\nu = 0.3$ , respectively. The non-dimensional deflection is defined as  $w_1 = w/h$  and the non-dimensional load is  $q_1 = qa^4/(Eh^4)$ . The boundary conditions of the

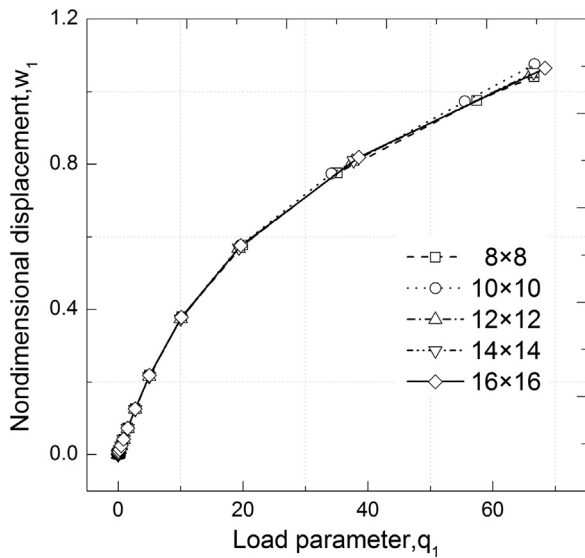


Fig. 3. Center deflection versus the uniformly distributed load for simply supported, isotropic, square plate with different nodes.

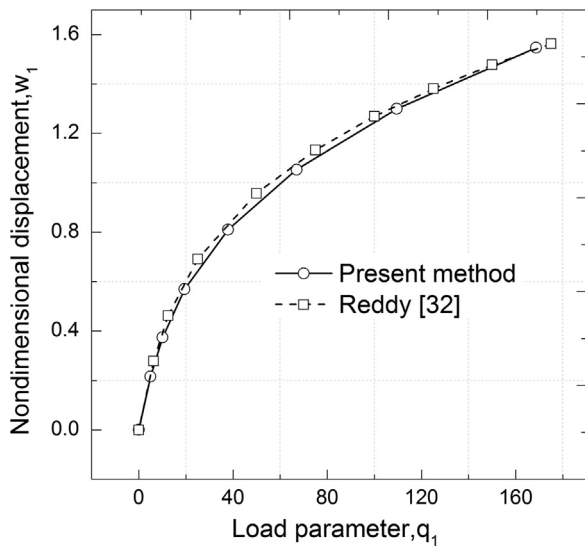


Fig. 4. Center deflection curves of an SSSS square isotropic plate under uniformly distributed load solved by different methods.

plate are simply supported for all four edges (SSSS). For comparison, we reduce the above Von Karman theory to classical plate theory which is also used by Reddy in that case. Fig. 3 depicts the nonlinear large deformation response for different nodes. Comparisons between the deflection–load curves solved by the present method and by the finite element method are shown in Fig. 4. From Figs. 3 and 4, we can see that it is suitable to set the particle distribution as  $16 \times 16$ , and that the agreement is reasonably good, although a slight difference exists between the solutions.

#### 4.2. Numerical cases

Fig. 5 illustrates the SLGSs under uniformly circular distributed transverse loads. The radius of the circle is  $R$ . To examine the influence of  $R$  on the nonlinear large deformation response of SLGSs, a case study is carried out on a square SLGS with the following geometrical and material properties

$$a = b = 15 \text{ nm}, h = 0.34 \text{ nm}, E = 1.02 \text{ Tpa}, \nu = 0.16.$$

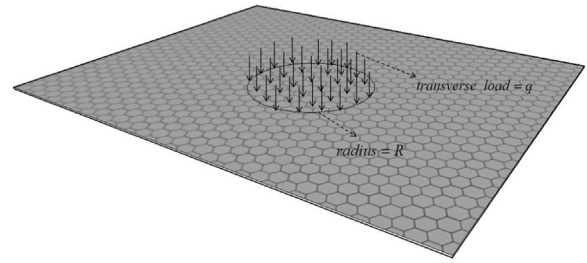


Fig. 5. SLGSs with uniformly circular distributed transverse loads.

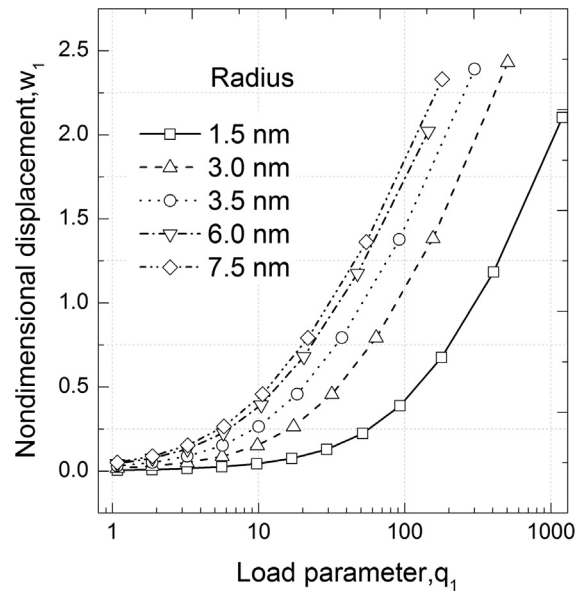


Fig. 6. Center deflection versus uniformly circular distributed load of the SSSS square SLGSs for different radii.

For boundary conditions of the four sides of the SLGSs, a sequence of letters containing “S” and “C” is used to denote simply supported (S) and fully clamped (C), respectively. The boundary conditions are given as follows:

- Simply supported (S): outside-layer nodes along the  $X$  axis,  $u_0 = w_0 = 0$ , outside-layer nodes along the  $Y$  axis,  $v_0 = w_0 = 0$ ; and
- Clamped (C): both the outside-layer nodes and the adjacent inside-layer nodes are set to be “S” to simulate the “C” [37].

Figs. 6–8 plot the center deflection curves of the SLGSs for SSSS, CSCS and CCCC boundary conditions, respectively. It is shown that, for specific boundary conditions, the center deflection increases with the increasing of the load radius  $R$ . It can also be found that, for an identical load radius and load value, the center deflection decreases following the sequence of the boundary conditions SSSS, CSCS and CCCC. As a result of this, there is an increase in edge constraints as the boundary conditions shift from SSSS to CSCS to CCCC.

The aspect ratio, which is defined as width/length, also influences the nonlinear large deformation response of SLGSs. SLGSs with a constant length  $a = 15 \text{ nm}$  and variable width (i.e. variable aspect ratios) are simulated to study the influence of aspect ratio on the nonlinear behavior of SLGSs. Figs. 9–11 display center deflection variation along with the variation of uniformly distributed load for different aspect ratios of SSSS, CSCS and CCCC SLGSs, respectively. As we can see from Fig. 9, center displacement

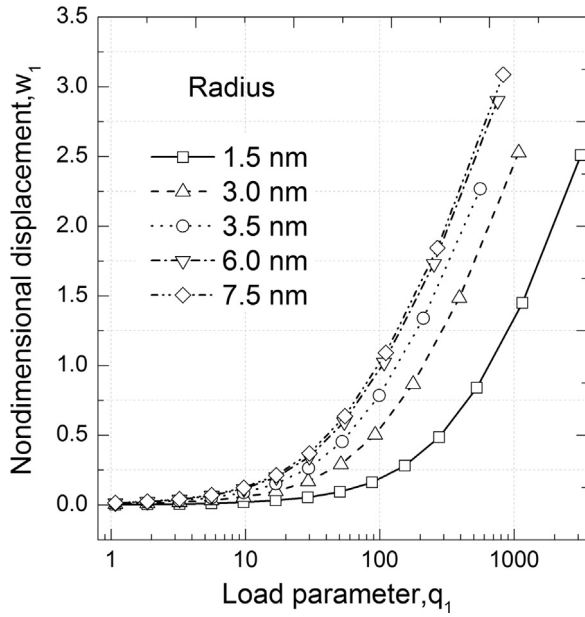


Fig. 7. Center deflection versus uniformly circular distributed load of the CSCS square SLGSs for different radii.

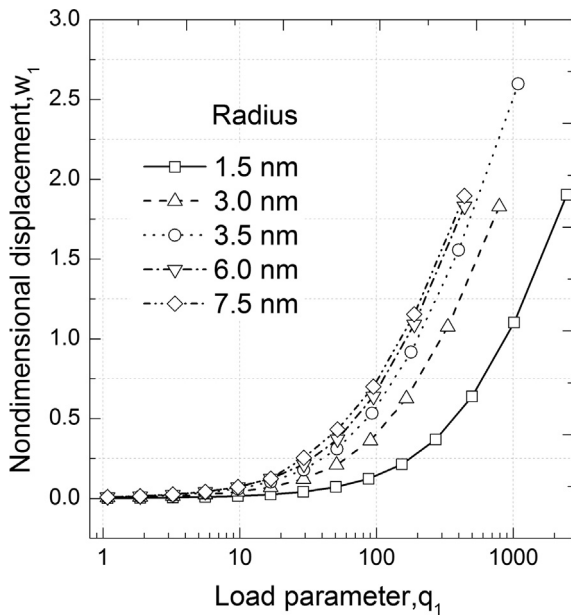


Fig. 8. Center deflection versus uniformly circular distributed load of the CCCC square SLGSs for different radii.

increases with the increasing of aspect ratio for specific loads. Similar observations are found in Figs. 10 and 11. In comparing Figs. 9–11, it can be concluded that the boundary conditions can be ranked as CCCC, CSCS and SSSS in descending order of the enhancement effect. In order to examine the influence of side length on the nonlinear large deformation response of SLGSs, we simulate isotropic, square SLGSs with different side lengths. Five values of side length are taken: 10 nm, 15 nm, 20 nm, 25 nm and 30 nm. All of these simulated SLGSs are subjected to transverse load uniformly distributed on the whole area. We define another nondimensional load  $q_2 = q \times 10^6 / E$  to demonstrate the impact of the side length on the nonlinear large deformation response clearly. The variation trend of the center deflection, along with the increase in uniformly distributed loads of SSSS SLGSs for different side lengths, is plotted in Fig. 12–14 present the same variation

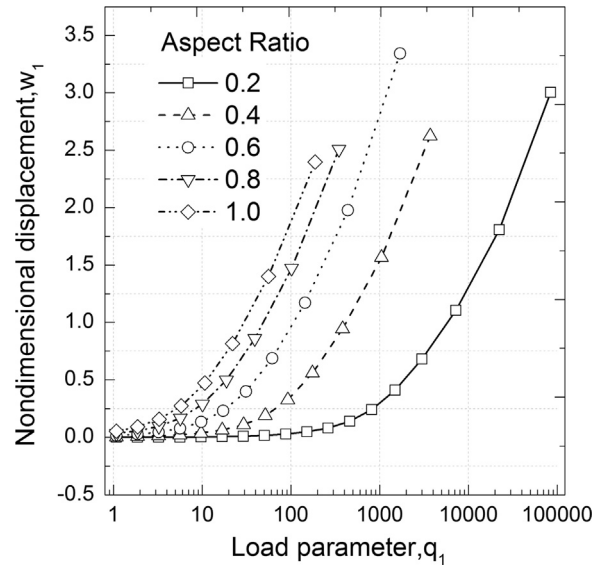


Fig. 9. Center deflection versus uniformly distributed load of the SSSS SLGSs for different aspect ratios.

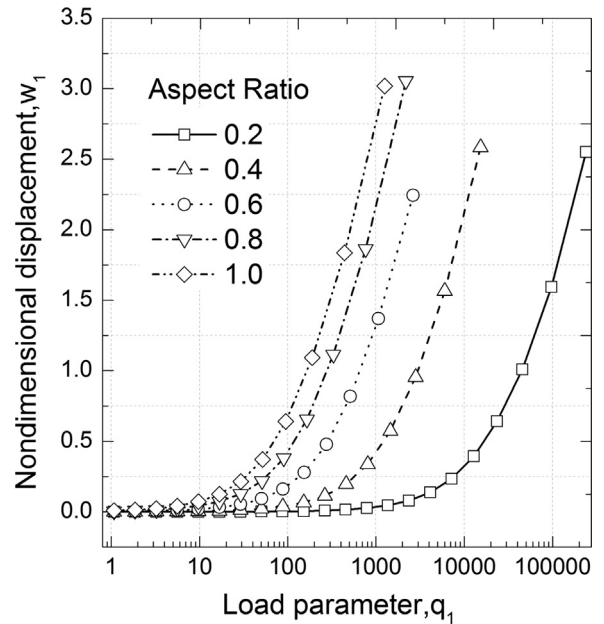


Fig. 10. Center deflection versus uniformly distributed load of the CSCS SLGSs for different aspect ratios.

trend of center deflection of CSCS and CCCC SLGSs, respectively. It is evident from the results that, for specific load and boundary conditions, as the side length increases, the center displacement increases. These curves also indicate that the constraint effects of these three kinds of boundary conditions can be ranked as CCCC, CSCS and SSSS in descending order.

It is worth considering nonlocal parameters in simulating nanostructures, as they have a manifest influence on the mechanical behaviors of small-size structures. To examine such influences, we simulate isotropic, square SLGSs with constant side lengths of 15 nm and consider only CCCC boundary conditions. We assume that the transverse load applied to the SLGSs has the following mathematical expression

$$q = q_0 e^{kx} \quad (44)$$

In addition, the corresponding nondimensional load is defined as  $q_1 = q_0 a^4 / (Eh^4)$ . Three cases are studied, i.e. (1)  $k = 0.5 \times 10^8$ ;

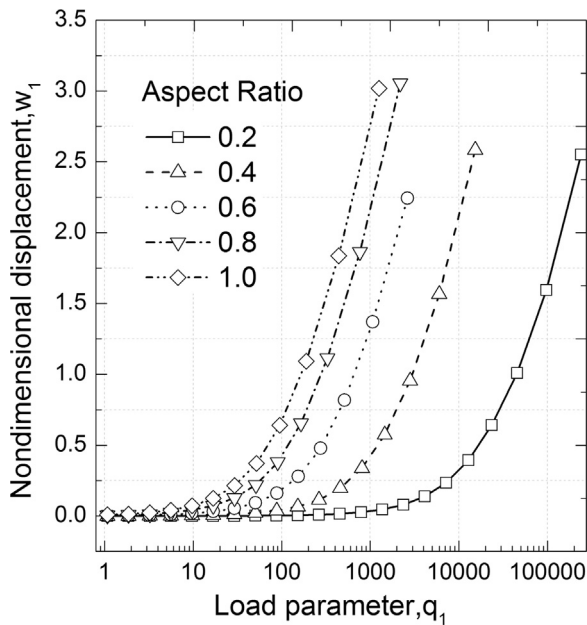


Fig. 11. Center deflection versus uniformly distributed load of the CCCC SLGSs for different aspect ratios.

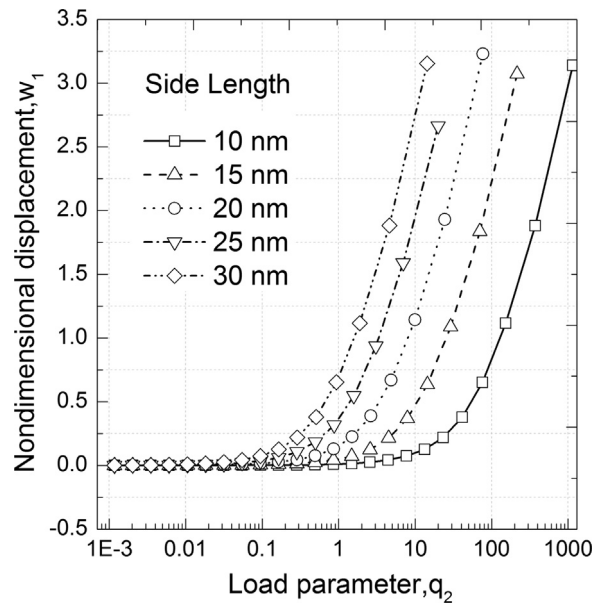


Fig. 13. Center deflection versus uniformly distributed load of the square CCCC SLGSs for different side lengths.

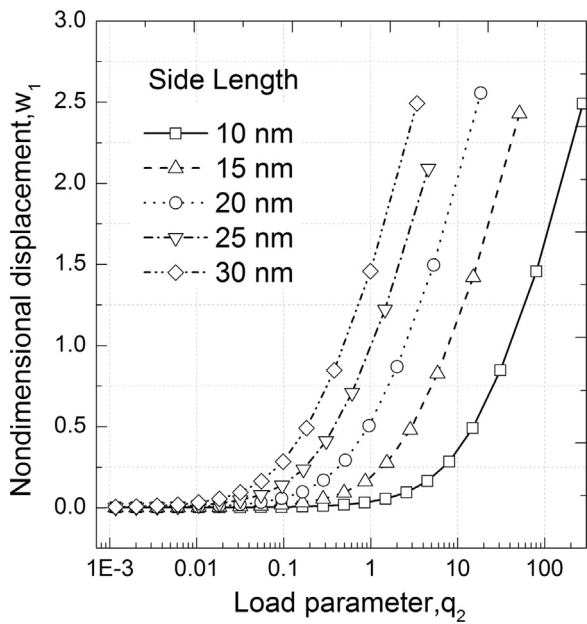


Fig. 12. Center deflection versus uniformly distributed load of the square SSSS SLGSs for different side lengths.

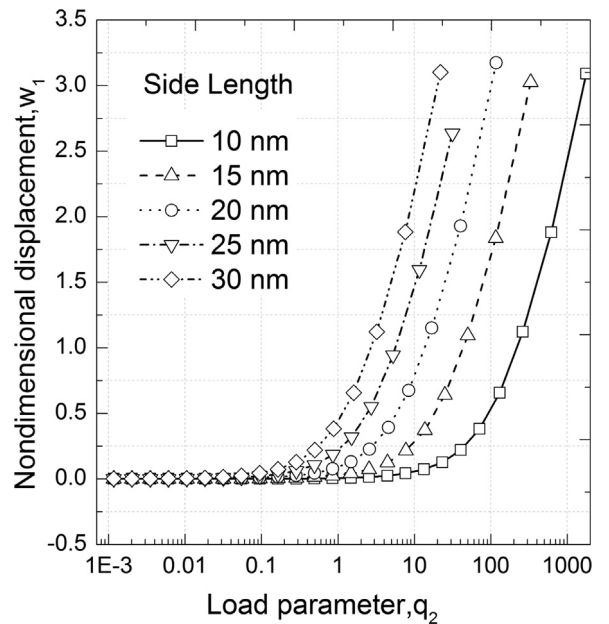


Fig. 14. Center deflection versus uniformly distributed load of the square CCCC SLGSs for different side lengths.

(2)  $k = 2 \times 10^8$ ; and (3)  $k = 3.5 \times 10^8$ . Corresponding to these three cases, the plots of center deflection versus transverse load for different nonlocal parameters are shown in Figs. 15–17, respectively. Taking Fig. 17 as an example, it can be seen that the center deflection decreases as the nonlocal parameter increases. The same phenomenon can be observed from Figs. 15 and 16, although the trend is less obvious than in Fig. 17. When we consider the different values of  $k$  in these three figures, we can draw the conclusion that the larger the values of  $k$ , the more remarkable the influence of nonlocal parameters on the nonlinear large deformation response is. This phenomenon is consistent with Eq. (31).

### 5. Conclusions

In this paper, the element-free kp-Ritz method has been applied for the geometrically nonlinear analysis of SLGSs. The mechanical behavior is described using the classical plate theory combined with the nonlocal elasticity theory, which has the ability to capture the small size effect. Based on total Lagrangian formulation, the system nonlinear equations are derived from the Ritz procedure. The equations are then solved using the modified Newton–Raphson method and arc-length continuation. Comparison study shows that the results are in excellent agreement with those reported by previous researchers, indicating that the element-free kp-Ritz method is efficient in solving large deformation problems. Many numerical studies are conducted to examine the influence of boundary conditions, aspect ratio, side

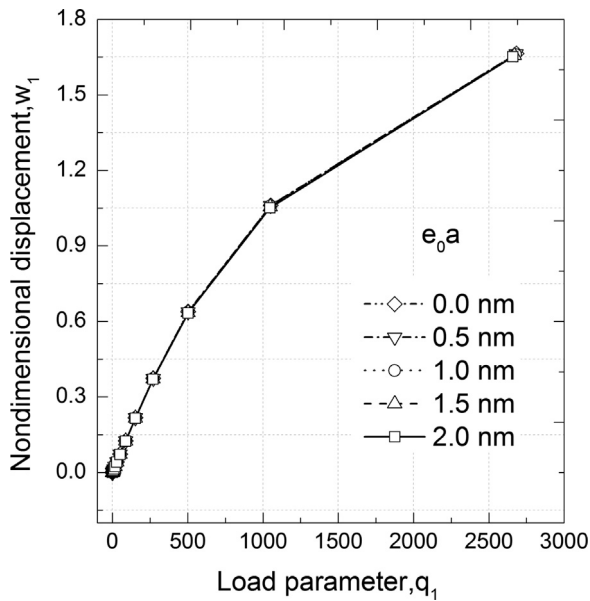


Fig. 15. Center deflection versus exponentially distributed load of the square CCCC SLGSs for different nonlocal parameters ( $k = 0.5 \times 10^8$ ).

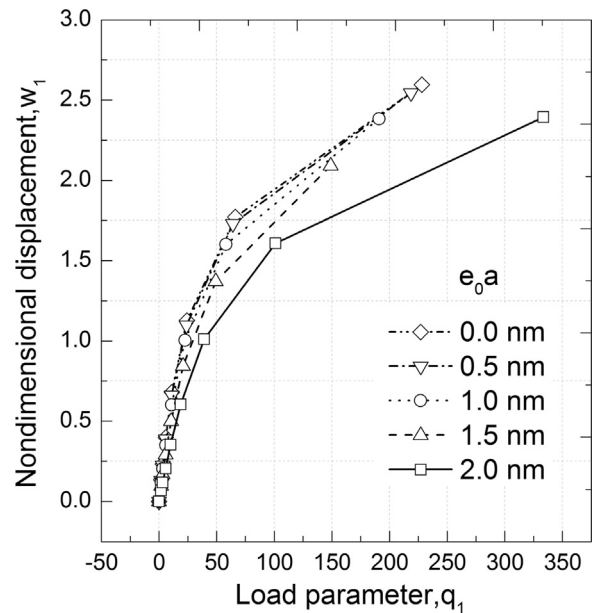


Fig. 17. Center deflection versus exponentially distributed load of the square CCCC SLGSs for different nonlocal parameters ( $k = 3.5 \times 10^8$ ).

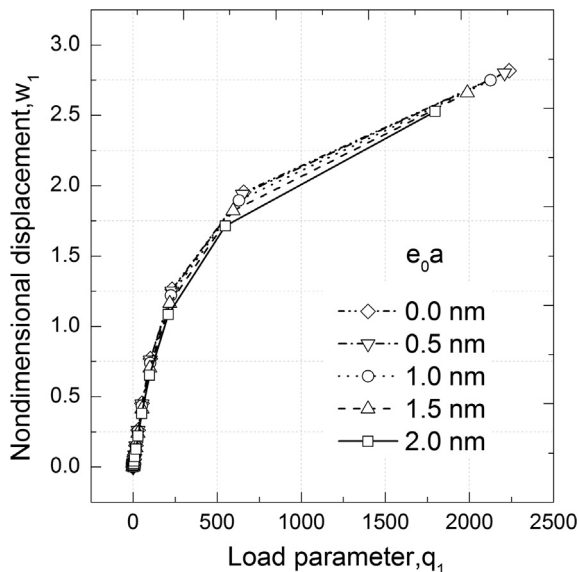


Fig. 16. Center deflection versus exponentially distributed load of the square CCCC SLGSs for different nonlocal parameters ( $k = 2 \times 10^8$ ).

length and nonlocal parameters on the nonlinear large deformation response of SLGSs.

## Acknowledgments

The work described in this paper was fully supported by grants from the Research Grants Council of the Hong Kong Special Administrative Region, China (Project no. 9042047, CityU 11208914) and the National Natural Science Foundation of China (Grant nos. 11402142 and 51378448).

## References

[1] K.S. Novoselov, A.K. Geim, S.V. Morozov, D. Jiang, Y. Zhang, S.V. Dubonos, I. V. Grigorieva, A.A. Firsov, Electric field effect in atomically thin carbon films, *Science* 306 (2004) 666–669.

[2] A. Sakhaee-Pour, Elastic properties of single-layered graphene sheet, *Solid State Commun.* 149 (2009) 91–95.

[3] F. Scarpa, S. Adhikari, A.S. Phani, Effective elastic mechanical properties of single layer graphene sheets, *Nanotechnology* 20 (2009) 065709.

[4] C. Gómez-Navarro, R.T. Weitz, A.M. Bittner, M. Scolari, A. Mews, M. Burghard, K. Kern, Electronic transport properties of individual chemically reduced graphene oxide sheets, *Nano Lett.* 7 (2007) 3499–3503.

[5] P. Lehtinen, A. Foster, A. Ayuela, A. Krasheninnikov, K. Nordlund, R. Nieminen, Magnetic properties and diffusion of adatoms on a graphene sheet, *Phys. Rev. Lett.* 91 (2003) 017202.

[6] O.A. Shenderova, V.V. Zhirnov, D.W. Brenner, Carbon nanostructures, *Crit. Rev. Solid State Mater. Sci.* 27 (2002) 227–356.

[7] C. Tang, L. Meng, L. Sun, K. Zhang, J. Zhong, Molecular dynamics study of ripples in graphene nanoribbons on 6H-SiC(0001): temperature and size effects, *J. Appl. Phys.* 104 (2008).

[8] A. Brodka, J. Koloczec, A. Burian, Application of molecular dynamics simulations for structural studies of carbon nanotubes, *J. Nanosci. Nanotechnol.* 7 (2007) 1505–1511.

[9] Y. Chandra, R. Chowdhury, F. Scarpa, S. Adhikari, Vibrational characteristics of bilayer graphene sheets, *Thin Solid Films* 519 (2011) 6026–6032.

[10] A. Krishnan, E. Dujardin, T.W. Ebbesen, P.N. Yianilos, M.M.J. Treacy, Young's modulus of single-walled nanotubes, *Phys. Rev. B* 58 (1998) 14013–14019.

[11] B.I. Yakobson, C.J. Brabec, J. Bernholc, Nanomechanics of carbon tubes: instabilities beyond linear response, *Phys. Rev. Lett.* 76 (1996) 2511–2514.

[12] A.C. Eringen, On differential equations of nonlocal elasticity and solutions of screw dislocation and surface waves, *J. Appl. Phys.* 54 (1983) 4703–4710.

[13] A.C. Eringen, *Nonlocal Polar Field Models*, Springer, Berlin, 1976.

[14] J. Peddieson, G.R. Buchanan, R.P. McNitt, Application of nonlocal continuum models to nanotechnology, *Int. J. Eng. Sci.* 41 (2003) 305–312.

[15] Q. Wang, Wave propagation in carbon nanotubes via nonlocal continuum mechanics, *J. Appl. Phys.* 98 (2005).

[16] B. Arash, Q. Wang, K.M. Liew, Wave propagation in graphene sheets with nonlocal elastic theory via finite element formulation, *Comput. Methods Appl. Mech. Eng.* 223–224 (2012) 1–9.

[17] S. Rouhi, R. Ansari, Atomistic finite element model for axial buckling and vibration analysis of single-layered graphene sheets, *Phys. E: Low-dimens. Syst. Nanostruct.* 44 (2012) 764–772.

[18] Y. Zhang, Z.X. Lei, L.W. Zhang, K.M. Liew, J.L. Yu, Nonlocal continuum model for vibration of single-layered graphene sheets based on the element-free kp-Ritz method, *Eng. Anal. Bound. Elements* 56 (2015) 90–97.

[19] Y. Zhang, L.W. Zhang, K.M. Liew, J.L. Yu, Transient analysis of single-layered graphene sheet using the kp-Ritz method and nonlocal elasticity theory, *Appl. Math. Comput.* 258 (2015) 489–501.

[20] P. Zhu, L.W. Zhang, K.M. Liew, Geometrically nonlinear thermomechanical analysis of moderately thick functionally graded plates using a local Petrov-Galerkin approach with moving Kriging interpolation, *Compos. Struct.* 107 (2014) 298–314.

[21] L.W. Zhang, P. Zhu, K.M. Liew, Thermal buckling of functionally graded plates using a local Kriging meshless method, *Compos. Struct.* 108 (2014) 472–492.

[22] L.W. Zhang, Z.X. Lei, K.M. Liew, J.L. Yu, Static and dynamic of carbon nanotube reinforced functionally graded cylindrical panels, *Compos. Struct.* 111 (2014) 205–212.

- [23] L.W. Zhang, Z.X. Lei, K.M. Liew, J.L. Yu, Large deflection geometrically nonlinear analysis of carbon nanotube-reinforced functionally graded cylindrical panels, *Comput. Methods Appl. Mech. Eng.* 273 (2014) 1–18.
- [24] J.W. Yan, L.W. Zhang, K.M. Liew, L.H. He, A higher-order gradient theory for modeling of the vibration behavior of single-wall carbon nanocones, *Appl. Math. Model.* 38 (2014) 2946–2960.
- [25] Z.X. Lei, L.W. Zhang, K.M. Liew, J.L. Yu, Dynamic stability analysis of carbon nanotube-reinforced functionally graded cylindrical panels using the element-free kp-Ritz method, *Compos. Struct.* 113 (2014) 328–338.
- [26] X. Zhao, K.M. Liew, Geometrically nonlinear analysis of functionally graded plates using the element-free kp-Ritz method, *Comput. Methods Appl. Mech. Eng.* 198 (2009) 2796–2811.
- [27] A. Naderi, A.R. Saidi, Nonlocal postbuckling analysis of graphene sheets in a nonlinear polymer medium, *Int. J. Eng. Sci.* 81 (2014) 49–65.
- [28] E. Jomehzadeh, A.R. Saidi, A study on large amplitude vibration of multi-layered graphene sheets, *Comput. Mater. Sci.* 50 (2011) 1043–1051.
- [29] H.S. Shen, L. Shen, C.L. Zhang, Nonlocal plate model for nonlinear bending of single-layer graphene sheets subjected to transverse loads in thermal environments, *Appl. Phys. A* 103 (2011) 103–112.
- [30] W.H. Duan, C.M. Wang, Nonlinear bending and stretching of a circular graphene sheet under a central point load, *Nanotechnology* 20 (2009) 7.
- [31] E. Jomehzadeh, M.K. Afshar, C. Galiotis, X. Shi, N.M. Pugno, Nonlinear softening and hardening nonlocal bending stiffness of an initially curved monolayer graphene, *Int. J. Non-Linear Mech.* 56 (2013) 123–131.
- [32] M. Amabili, *Nonlinear Vibrations and Stability of Shells and Plates*, Cambridge University Press, New York, 2008.
- [33] K.M. Liew, J. Wang, M.J. Tan, S. Rajendran, Nonlinear analysis of laminated composite plates using the mesh-free kp-Ritz method based on FSDT, *Comput. Methods Appl. Mech. Eng.* 193 (2004) 4763–4779.
- [34] M. Fafard, B. Massicotte, Geometrical interpretation of the arc-length method, *Comput. Struct.* 46 (1993) 603–615.
- [35] M.A. Crisfield, *Non-Linear Finite Element Analysis of Solids And Structures*, John Wiley and Sons, Chichester, UK, 1991.
- [36] J.N. Reddy, *Mechanics of Laminated Composite Plates and Shells: Theory and Analysis*, 2nd ed., CRC Press, Boca Raton, 2004.
- [37] R. Ansari, S. Sahmani, B. Arash, Nonlocal plate model for free vibrations of single-layered graphene sheets, *Phys. Lett. A* 375 (2010) 53–62.